Working characteristics of self-pitching flapping foil propulsor

MARINE 2021

Lei Mei [1], Wenhui Yan[2]，Junwei Zhou[1*]，Dong Yu[1] and Pengcheng Wu[1]

[1] Harbin Institute of Technology (Weihai), No. 2 Wenhua West Road, Weihai City, Shandong Province, China.E-mail: meilei@hit.edu.cn, zhoujunweihit@foxmail.com,

[2] North China University of Technology, 5 Jinyuanzhuang Road, Shijingshan District, Beijing City, China.Email: abuaa@163.com

[*] Corresponding author: Third Author, zhoujunweihit@foxmail.com

ABSTRACT

This work investigates the working characteristics of a large amplitude semi-passive flapping-foil with a prescribed sinusoidal heave motion and a passive pitch motion. Different from the active flapping foil with two degrees of freedom, this self-pitching flapping foil (SPFF) constructs a single degree of freedom spring mass system in the direction around the pitching motion axis. Because of the torsion spring attached to the foil, this kind of foil is a flow-induced vibration system, and the torsional spring stiffness, the foil inertia and the hydrodynamic added inertia should affect the propulsive performance. Its working characteristics are affected by two non-dimensional coeffificients: the frequency ratio r and spring stiffness ratio k' according to dimensional analysis. In this paper, the fluid-structure coupling method is used to analyze the working characteristics of the self-pitching flapping foil with different parameter settings. After the verification of the numerical method, the investigation first discusses the working characteristics of the self-pitching flapping foil when the system resonates and identifies that the resonance can make the self-pitching flapping foil deviate from the ideal angle of attack, and its fluctuation of short-term average thrust coefficient becomes irregular. That leads to the performance degradation of self-pitching flapping foil and even the loss of propulsion ability. Then the influence of frequency ratio on the propulsive performance is investigated. The numerical results confirm that the semi-active flapping foil performs efficiently when the frequency ratio r is small, and the maximum efficiency can reach as high as 86%; the more suitable frequency ratio is recommended to be less than 0.5. Finally, the effect of spring stiffness ratio is discussed under a small frequency ratio. The results imply that the peak efficiency of self-pitching flapping foil is not monotonic with different spring stiffness ratio, and there is a maximum value; but self-pitching flapping foil can maintain the peak efficiency over a wider range of spring stiffness ratio, the range is 0.1 ~ 1000 in this report; Through the analysis of the performance curves of the foil with different pitching center positions, it indicates that the influence trend of pitching center position is close to that of the spring stiffness ratio.

Keywords: Self-pitching; Flapping foil propulsor; Ratio of frequency; Torsion spring stiffness.

1. INTRODUCTION

In order to achieve high efficiency and maneuverability of underwater vehicles, a variety of flapping foil propulsors were designed, which take inspiration from the flap fins swimming of fish, the flap wings locomotion of birds, and the flap limbs glide of turtles. Up to now, the flapping foil propulsors have been a very active research field(Wu *et al.*2020). A typical flapping foil propulsor is a rigid flapping foil with two degrees of freedom, which is composed of simple harmonic heave motion and pitch motion (Anderson *et al.*1998). The pitch motion is usually 90 degrees behind the heave motion. In the study of flapping foil motion, researchers have refined many key parameters, such as St number (Taylor *et al.*2003; Guglielmini *et al.* 2004; Floc'h *et al.*2012), heave amplitude ratio and pitch angle. In the research of traditional propeller, the performance parameters are usually defined as the function of the advance coefficient, so some researchers used the advance coefficient J to replace the St number (Floc'h *et al.*2012; Hopper 1989; Thawewat *et al.*2018;

Li *et al.* 2019) in the study of the performance of the flapping foil, which is reciprocal to the St number. Many studies have shown that in the range of St number from 0.2 to 0.4, the flapping foil has higher efficiency [Taylor *et al.*2003;Thawewat *et al.*2018]. The research on the heave amplitude ratio and pitch angle shows that when the heave amplitude ratio is below 3, the efficiency increases with the increase of the ratio of heave amplitude[Guglielmini *et al.* 2004]; The effects of Read (2003), Schouveiler (2005)and Floryan (2017) on pitch angle were also studied. In addition, many scholars have studied the phase difference and the position of the rotation axis of the foil (Guglielmini *et al.* 2004; Lin *et al.* 2019), the shape of the motion curve of the foil (Esfahani *et al.*2015;Teng *et al.*2016; karbasian *et al.*2017), etc. From many studies, the highest efficiency of the two degree of freedom rigid wing has reached about 87% (Anderson *et al.*1998;Li *et al.* 2019; Zhang *et al.* 2012).

At the same time, some studies have also reminded the disadvantages of the fully prescribed flapping foil propulsion, e.g., strong forces fluctuation and mechanical complication since it requires mechanically coupled and constrained the two motions through complex mechanisms. However, several issues can arise from this complexity. First, a significant amount of energy could be lost due to the friction between the different moving components. Moreover, complex mechanical system are usually prone to a higher risk of failure in addition to being more expensive. Compared with the two degree of freedom flapping foil, the mechanism of single degree of freedom flapping foil is much simpler, but the efficiency of this kind of flapping foil is much lower (Andersen *et al.*2017; Koochesfahani*et al.*1989; Schnipper *et al.*2009). Another possible way to resolve this drawback is to use the semiactive flapping foil for which only one actuator is required (Kim *et al.*,2017). In many studies, one freedom motion (usually the heave motion) of the foil is usually prescribed , while the pitch motion is determined by a spectial structure or material. While ensuring the high efficiency of propulsion, the semiactive propulsion system, therefore, promises a more feasible approach in engineering project compared to fully prescribed motions foil system. There are three kinds of implementation methods. The first method is to control the pitch motion of the flapping foil by adding a self-rectifying rotation structure, so that the foil can work at a certain range of pitching angle (Joe *et al.* 2017). The second one is to use the torsion spring on the foil to control the pitch motion, also known as self-pitching flapping foil (spff), or semi-active flapping foil. When the foil is pitching under the action of hydrodynamic moment, it's pitching angle is determined by torsion spring force, hydrodynamic force and inertial force, so that it can work at a certain angle of attack (Thawewat *et al.*2018;Bøckmann*et al.* 2014;Yang *et al.*2018). The last one is the flexible foil used by Dewey (2013],) bourlet (2015), cleaver (2016), Lee (2018) and Liu (2016)etc. Although the flexible foil does not have pitching motion, due to the flexibility of the material, this kind of foil can deform under the action of hydrodynamic force.So it also has a equivalent pitching angle and can adapt to different working conditions.

From the point of view of few control parameters and easy realization of mechanism, SPFF is a better choice among the three design methods, which has also attracted more and more attention. In order to realize the design of torsion spring, BøCkmann (2014) used the piano wire which could slide and rotate freely to connect the foil and the bracket, and adjusted the equivalent torsion spring stiffness by changing the connection position; Yang (2018) realized the equivalent torsion spring stiffness by a tension spring with a certain force arm. Thaweewat (2018) constructed dimensionless frequency ratio and dimensionless spring stiffness ratio, and used numerical method to discuss the influence of flapping ratio , St number (or advance ratio), heave motion trajectory and other parameters on the propulsive performance of spff. Veilleux et al. (2017) and Boudreau et al. (2018) adapted fully-passive flapping-foil in hydrokinetic turbine, that is, both degrees of freedom are decoupled and elastically supported by springs, and the system can work continuously and achieve energy extraction.

As reviewed above, due to the introduction of the spring, the spring force, mass force and hydrodynamic force constitute a new spring-mass system. Compared with the flapping foil with given two coupled and constrained motions, the performance of the SPFF is obviously different. Meanwhile, there are more parameters affecting the performance of SPFF. It is lack of comprehensive parametric analysis to conclude the theoretical maximum efficiency. In view of this, based on the work of Thaweewat (2018), more Systematic and parametric analysis will be conducted to correlate the influencing factors to the propulsive of SPFF in this research, and the fluid-structure coupling method based on viscous flow CFD is used to simulate the flow field and dynamic working process, so as to more accurately simulate the separation phenomenon. Firstly, this paper introduces the motion law of the SPFF and the spring mass system. And some parameters are defined; Then, the fluid-structure coupling numerical method is described and verified; Finally, the related results and the analysis of a

parametric study are presented and the current study also evaluates the sensitivity of the performance to the variation of several governing parameters.

2. DEFINITION OF FLAPPING FOIL MOTION

In this paper, a rigid two-dimensional NACA 0012 airfoil is used, as shown in Fig.1. The flapping foil propulsor with a chord length, c, performs a combined pitch and heave motion with an advancing velocity V_A (m/s), a period T (s) and a heave height B (m). The foil is subjected to heave vertically with a simple harmonic function at its pivot point, which is expressed in Equation 1. Nevertheless, unlike the flapping foil with given heave and pitch motion, the pitching motion of SPFF is controlled by a torsion spring attached to the foil as illustrated in Fig. 2. Consequently, the sinusoidal heave motion together with the advance velocity creates an oscillating hydrodynamic force and moment causing the foil to to work at an angle of attack α (AoA). But the torsion spring is used to restore the foil toward the horizontal plane. Under the combined action of this hydrodynamic moment and torsion spring, the flapping foil produces a pitching angle θ. The pitching center is in a distance, C_0, from the leading-edge of the foil.

Heave motion: $$y = y_0 \sin(2\pi f t) \qquad \textit{Equation 1}$$

where y_0 is the heave amplitude, m; f is the flapping frequency, Hz; and t is the time, s.

In operation, the SPFF is affected by the combined action of inertia moment in the pitching direction, spring moment, and hydrodynamic moment, and the dynamic equation of the flapping foil can be written as follows

$$I\ddot{\theta} + K\theta = M_h \qquad \textit{Equation 2}$$

Where I is the foil moment of inertia, kg.m^2; K is torsion spring stiffness, N/m; M_h is the hydrodynamic moment on SPFF, N.m.

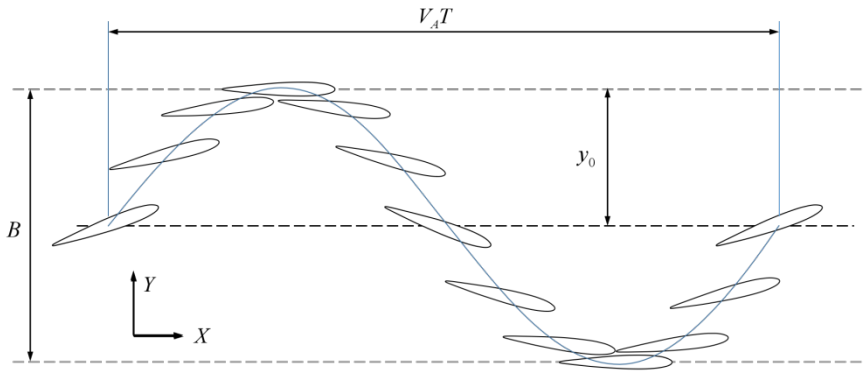

Figure 1. Sketch of the flapping foil propulsor, NACA0012, with combined motions.

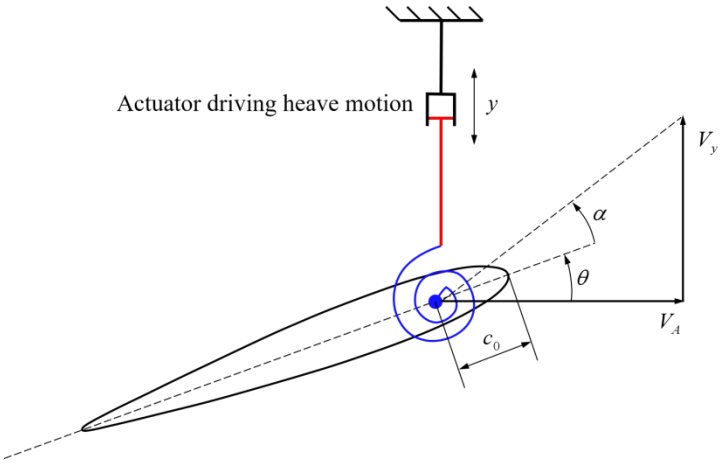

Figure 2. Schematic illustration of the SPFF with forced heave motion and attached torsion spring .

3. NONDIMENSIONAL PROPULSIVE INDICATORS

To study the flapping foil propulsion, some nondimensional parameters have been used in this paper. To nondimensionalize the flapping frequency, St Number is used, which is expressed as the following Equation 3.

$$\mathrm{St} = \frac{fB}{V_A} \qquad \textit{Equation 3}$$

Where $B=2y_0$ is heave height ,m;

For the convenience of comparing with marine propellers, Floc'h (Floc'h *et al.*, 2012) introduced the advance coefficient, J as shown in the Equation 4, which is inherited in this paper.

$$J = \frac{V_A}{fB} = \frac{1}{\mathrm{St}} \qquad \textit{Equation 4}$$

The Reynolds number of the flapping foil can be expressed as follow Equation 5.

$$\mathrm{Re} = \frac{fBc}{\upsilon}\sqrt{J^2+\pi^2} \qquad \textit{Equation 5}$$

Where v is the kinematic viscosity, m^2/s.

With reference to the work in Thaweewat *et al.*(2018), the dimensionless parameter spring stiffness ratio *K'* is defined to describe the spring stiffness. In the work of Thaweewat *et al.*(2018), the structure of spring stiffness ratio takes the planform area of hydrofoil as the reference area and the advance speed as the reference speed. This definition method makes it difficult to analyze some problem. For example, when the performance of the flapping foil with a certain spring stiffness ratio needs to be analyzed at different advance speed coefficients, advance speed should be changed as well as the spring stiffness. In addition, the reference speed in this definition method is inconsistent with the reference speed defined in the advance speed coefficient. And the reference area definition also inconsistent with the swept area used in traditional propeller Nondimensional

propulsive indicators. Therefore, taking *f***B* as the reference speed and the swept area *B***H* of the flapping foil as the reference area, the spring stiffness ratio *K'* is redefines in this paper as the following Equation 6:

$$K' = \frac{K}{\rho f^2 B^3 H c} \qquad \textit{Equation 6}$$

Where ρ is the density of water, g/cm; *H* is the span of the foil, m.

The definition of frequency ratio *r* in this paper is the same as that in Thaweewat *et al.*(2018). It is the spring coeffificient non-dimensionalized based on frequency namely force-to-natural frequency ratio. It can be expressed as follow Equation 7

$$r = \frac{f}{f_N} = 2\pi f \sqrt{\frac{I}{K}} \qquad \textit{Equation 7}$$

Where f_N is the natural frequency of the SPFF, Hz; *I* is the foil moment of inertia, kg.m^2.

4. NUMERICAL METHOD AND VALIDATION

4.1 Governing Equations

In this paper, the CFD software, FINE/Marine, is used to investigate the hydrodynamic performance of flapping foil propulsor. The hydrodynamic performance of the SPFF can be obtained by solving the fluid hydrodynamic equation and the rigid body dynamics equation simultaneously. This solver adopts internal implicit iteration within a time step iteration to ensure a strong and accurate flow/motion coupling. And the Menter's k-ω shear-stress transport turbulent model was used (Menter *et al.*, 1994). The hydrodynamic model uses the foil motion as its input to determine the hydrodynamic force and moment. As for the dynamic model, the hydrodynamic force and moment from the hydrodynamic model are applied in the Newton-Euler equation to determine the foil motion. The dynamic equation of SPFF has been introduced above in Equation 2. And by using integral incompressible viscous fluid dynamics equation, considering the motion of grid cells and without considering the influence of gravity, the hydrodynamic equation can be written as following Equation 13 and 14 :

$$\frac{\partial}{\partial t}\int_{\Omega} \rho d\Omega + \oint_{S} \rho(\vec{v} - \vec{v}_d)\cdot d\vec{S} = 0 \qquad \textit{Equation 2}$$

$$\frac{\partial}{\partial t}\int_{\Omega} \rho v_i d\Omega + \oint_{S} \rho v_i(\vec{v} - \vec{v}_d)\cdot d\vec{S} = \oint_{S} \tau_{ij} dS_j - \oint_{S} p d\vec{S} \qquad \textit{Equation 3}$$

Where Ω is the element volume; *v* is the flow velocity; v_d is the displacement velocity of element surface; τ is the viscous force and *P* is the pressure, Pa..

4.2 Mesh and method

In order to describe the motion of the SPFF accurately, the overlapping grid technique is used to construct the computational domain grid (background grid) and the airfoil domain grid(overlap grid) respectively. As shown in Fig. 3, the simulation is carried out in a computational domain of 40*c* × 80*c*, with overlapping domain of 2*c* × 1*c* around the foil in which the maximum mesh size is less than 1 / 2^8 of the chord length. Meanwhile, in order to accurately simulate the pressure and velocity gradient on the foil surface, as well as the separated

vortex in the trail, further mesh refinement is carried out on the foil surface and two regions(region I and region II). The size of the two refinement regions which are shown as blue and green rectangles is about 4*c*×5*c* and 5*c*×9*c* respectively. The near wall mesh is refined to ensure that the y+ value is about 1.0.

The boundary condition of foil surface is set as the non-slip wall boundary with wall functions to simulate the boundary layer flow. and the four outer boundaries of the foil domain region are defined as overlap grid boundaries. Four outside boundaries of the computational domain are set as far-field boundaries, in which the left, upper and lower boundaries are given velocity and pressure, and the right boundary velocity and pressure are extrapolated. The setting method of boundary conditions are shown in Fig. 3.

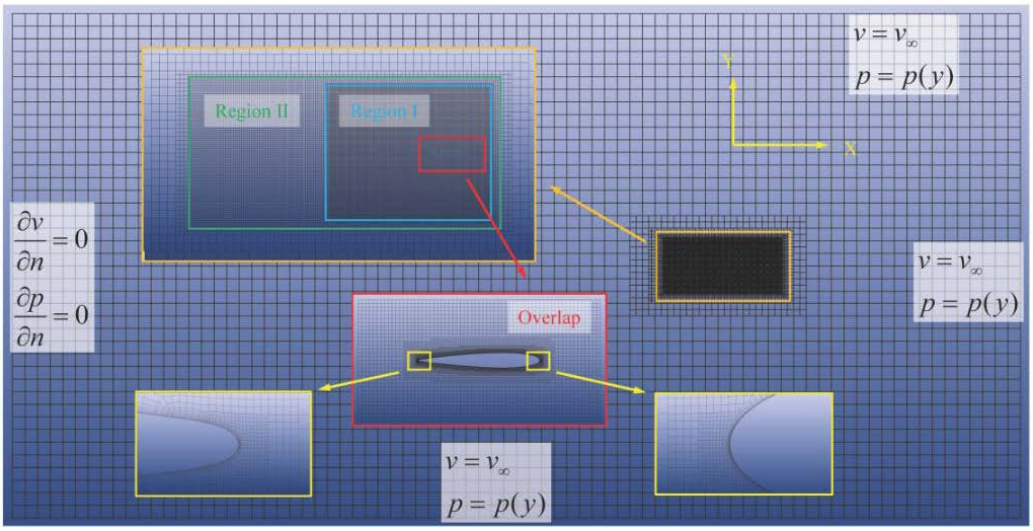

Figure 3. Schematic diagram of computational domain and gradual mesh refinement

4.3 Validation

In order to validate the numerical method used in the current work, three parts of validation are carried out in this part: the verification of grid independence, the verification of time step and turbulence model, and simulation verification of selected benchmark conditions in Anderson's (Anderson *et al.*, 1998) experiments.

First, grid independence validation was performed. Combined with the previous study, five sets of grids with different mesh refinement schemes were designed, and a better working condition was selected for grid independence validation. The grid size of these five mesh refinement scheme is shown in Table 1.

Table1. Grid size under five mesh refinement scheme

scheme	foil surface	region I	region II
Mesh 0	*c*/256	*c*/16	*c*/16
Mesh 1	*c*/128	*c*/16	*c*/16
Mesh 2	*c*/64	*c*/16	*c*/16
Mesh 3	*c*/256	*c*/32	*c*/16
Mesh 4	*c*/256	*c*/16	*c*/8

Under the selected working condition, the heave amplitude-to-chord ratio is y_0/c=2.5, the frequency ratio is r=0.2, and the spring stiffness ratio is K'=10. The time step $\Delta t/T$=0.001 is selected in the simulation. The

comparison of the results is shown in Fig. 4. It can be seen that the efficiency and thrust coefficient are similar in the five mesh refinement schemes. It means the influence of grid size on the flapping-foil efficiency and thrust coefficient is small. Only a few differences appear when advance coefficient J=2~6, and there is no obvious regularity. It is speculated that the fluctuation is caused by the unstable separated flow, and the detailed analysis will be introduced later. In order to give consideration to both computational efficiency and mesh refinement, Mesh 0 scheme will be selected for relevant simulation.

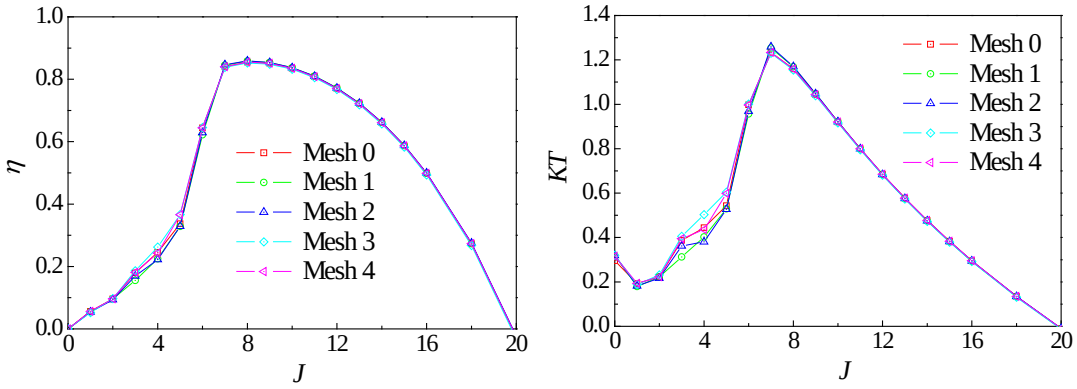

Figure 4. Comparison of foil performance under five mesh refinement scheme

The flow field formed by flapping-foil motion is a strong unsteady flow field accompanied by flow separation(Schouveiler *et al.*,2005; Andersen *et al.*,2017). Considering the influence of time step and turbulence model on the simulation accuracy of unsteady separated flow, comparative analysis of these two parameters is carried out.

At first, three time-step, $\Delta t/T$=0.0005, 0.001 and 0.002, are compared under the same working conditions as in grid validation. The k-ω turbulence model is used and the comparison results are shown in Fig.5. It can be seen that the efficiency and thrust curves of the flapping-foil almost coincide with each other under the two time-step settings of $\Delta t/T$=0.0005 and $\Delta t/T$=0.001; However when $\Delta t/T$ increases from 0.001 to 0.002, there are obvious differences in the performance curve, which is mainly reflected in the slight decrease of maximum efficiency and maximum thrust at the same time. Similar to the results of grid independence verification, the curves of efficiency and thrust coefficient fluctuate irregularly in the range of J = 2 ~ 6. Then, the k-ω turbulence model and IDDES (Gritskevich *et al.*, 2012) turbulence model are compared under the same conditions as the grid validation.The time step $\Delta t/T$ = 0.001 is used and the comparison results are shown in Fig.6. It is obvious that Menter's k-ω shear-stress transport turbulence model and Gritskevich's IDDES turbulence model are almost the same in the calculation of foil performance, only a few differences appear in the range of advance coefficient J=2~6. According to the comparison of the above time step and turbulence model, this paper finally selects the time step $\Delta t/T$=0.001 and the k-ω turbulence model for the following analysis.

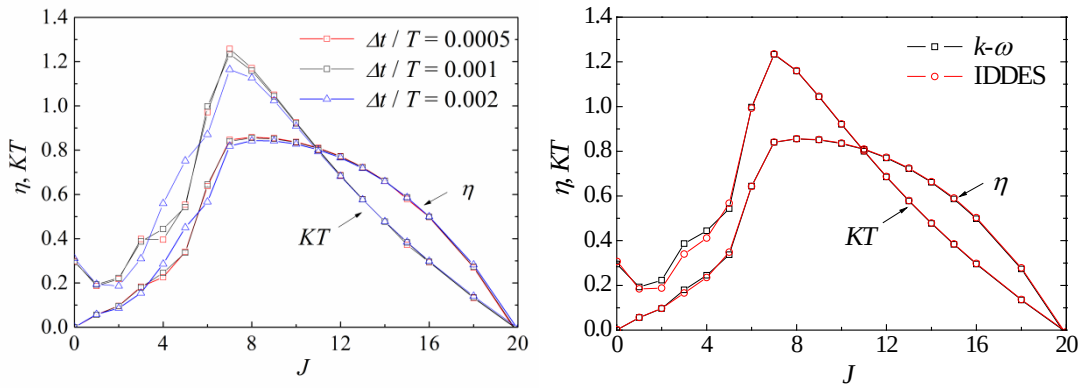

Figure 5 Comparison of propulsive performance with different time steps

Figure 6. Comparison of propulsive performance with different turbulence models

In the above verification, a common phenomenon is that the repeatability of performance parameters is poor in the range of J = 2 ~ 6. It is speculated that it may be caused by the large AOA and unstable separation on the foil surface.

In order to verify the conjecture, AoA curves and the vorticity field at the integral period are further compared under the four working conditions of J = 2, 4, 6 and J = 8 after the flow is fully developed, as shown in Fig. 7 and Fig. 8. It can be seen from Fig. 7 that the foil has an obvious separation vortex under the condition of J=2 and 4; The separation area becomes much smaller when advance coefficient J increase to 6; and there is no obvious separation phenomenon under the condition of J=8. The characteristics of the AOA curve inFig.8 are consistent with the phenomena described by the vorticity filed. the maximum AOA is about 48° under the condition of J= 2, and the maximum angle of attack is about 29° under the condition of J = 4, both of which have a too large AOA, corresponding to a large separation vortex; When advance coefficient J increases to 6, the maximum AOA decreases to about 19°. The AOA is still large, which corresponds to the separation of some regions on the foil surface; The maximum AOA is about 11.5° under the condition of J = 8, which decreases further and there is almost no separation on the foil surface. However, the AOA of flapping foil changes periodically, which is different from that of steady flow, the analysis of AOA here is only a preliminary discussion.

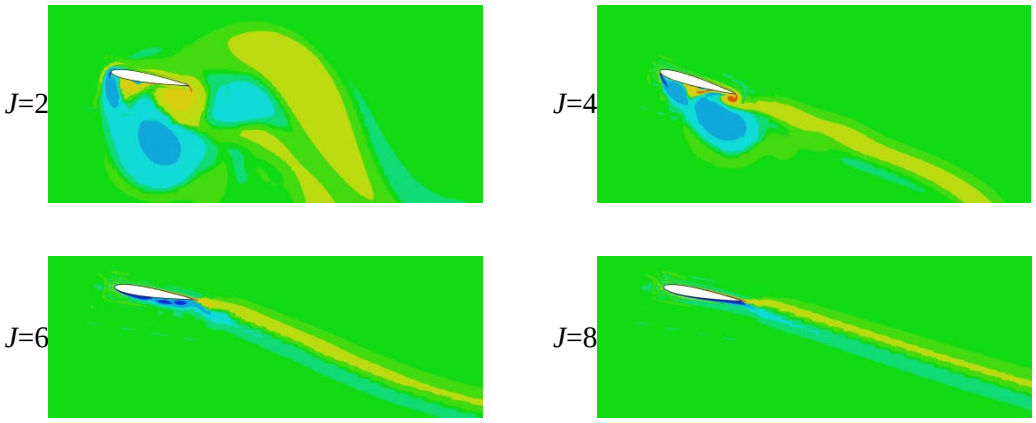

Figure 7. Comparison of separation vortex under different advance coefficients

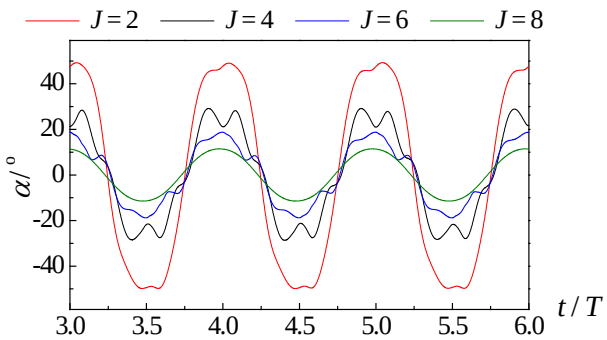

Figure 8. Comparison of AOA time-history curves under different advance coefficients

In addition to the vorticity nephogram, the convergence of the foil performance curve can also show the difference at low advance coefficients. The separation at low advance coefficient will lead to slow convergence and fluctuation in the convergence process. In order to describe the fluctuation, the average thrust coefficient

KT_a and the average efficiency η_a in one period are defined here. They are called short-time average thrust coefficient and short-time average efficiency, which are expressed respectively as follows:

$$KT_a(t_0) = \frac{1}{\rho f^2 B^3 H} \int_{t_0-T}^{t_0} F_x dt \qquad \textit{Equation 4}$$

$$\eta_a(t_0) = \frac{V_x \int_{t_0-T}^{t_0} F_x dt}{\int_{t_0-T}^{t_0} F_y V_y dt} \qquad \textit{Equation 5}$$

Fig. 9 and Fig.10 show the time-history curves of short-time average thrust coefficient KT_a and short-time average efficiency η_a under J=2、4、6、8. It can be seen that under the condition of J= 8, the performance curve of the foil will be stabilized quickly after roughly two cycles; The convergence of the performance curve is under the condition of J=2, which is roughly stabilized after 4 cycles; Under the condition of J=6, the convergence of performance curve is slower, showing a gradual convergence fluctuation but the fluctuation is not large; Under the condition of J=4, the performance curve of the foil show irregular fluctuations near a certain value. The irregular fluctuation phenomenon is consistent with the curve discrete performance near J=4 and J=6 in Fig.5 to Fig.7.

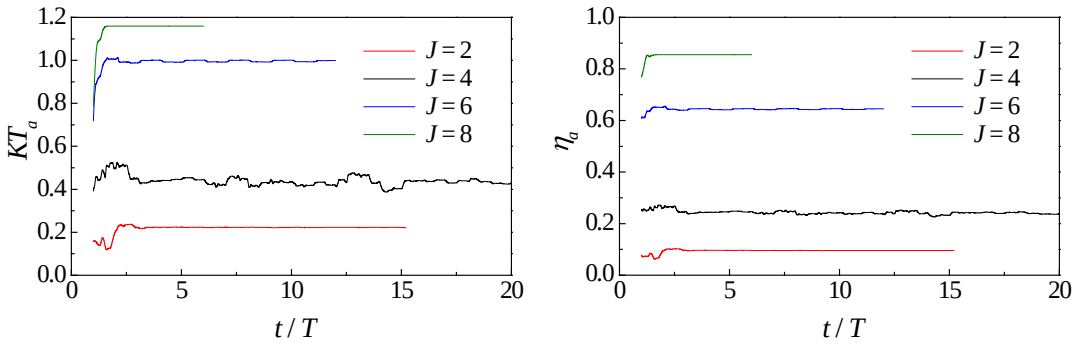

Figure 9. Short-time average thrust coefficient curves under different advance coefficients

Figure 10. Short-time average efficiency curves under different advance coefficients

At the end of this part, in order to validate the numerical method used in the current work, selected benchmark conditions in Anderson's (Anderson *et al.*, 1998) experiments are simulated, in which a rigid two-dimensional NACA 0012 airfoil is used. The heave amplitude-to-chord ratio is 0.75, and the pitching axis is 1 / 3 chord from the leading edge of the airfoil. The experimental and the calculated results are compared and shown in Fig. 11, which agrees with each other.

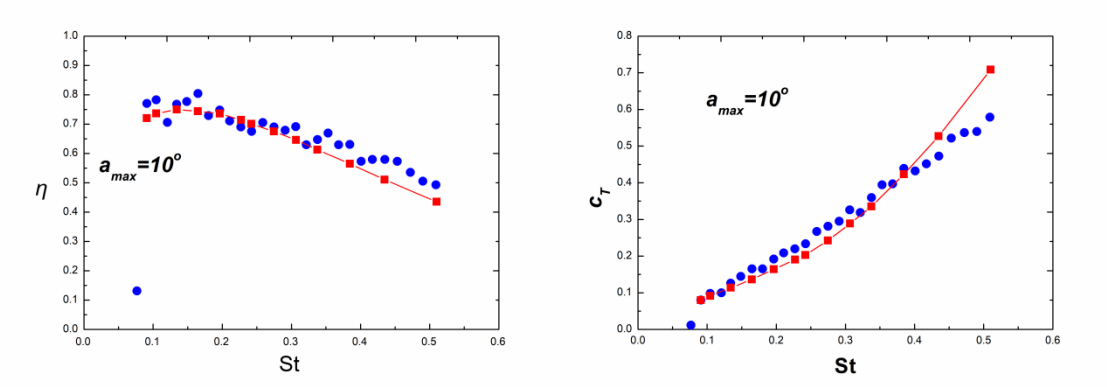

Figure11. Comparisons of the propulsive efficiency η and the thrust coefficient c_T with previous computational and experimental results (The red curve ■ is the CFD results of this paper, blue spot ● is the result of Anderson experiment)

5. RESULTS AND ANALYSIS

5.1 Effects of Frequency Ratio

According to the work of Thaweewat (2018), the system resonance will not have a good effect on the SPFF propulsion performance. However, in order to systematically study the performance of the SPFF, this paper first discusses the effect of resonance mechanism on the SPFF performance , then analyzes the performance of the foil under six frequency ratio *r*, and further studies the effect of frequency ratio on the performance of the foil.

Firstly, under the condition of heave amplitude-to-chord ratio y_0/c=2.5 and the spring stiffness ratio K'=10, the performance of the foil with the frequency ratio r=1.0 and r=0.2 is analyzed. Due to the influence of hydrodynamics, the natural frequency of SPFF may change slightly, but we still assume that when the frequency ratio r= 1.0, the system will resonate or approach the resonant state. In this paper, the resonance state is realized by adjusting the rotational inertia of foil. The short-time average thrust coefficient KT_a curves at four advance coefficients are shown in Fig.12. The selected four advance coefficients are J=0.002 (foil starting status), J=6 (a point in the rising section of the efficiency curve), J=8 (the maximum efficiency point) and J=15 (a point in the falling section of the efficiency curve).

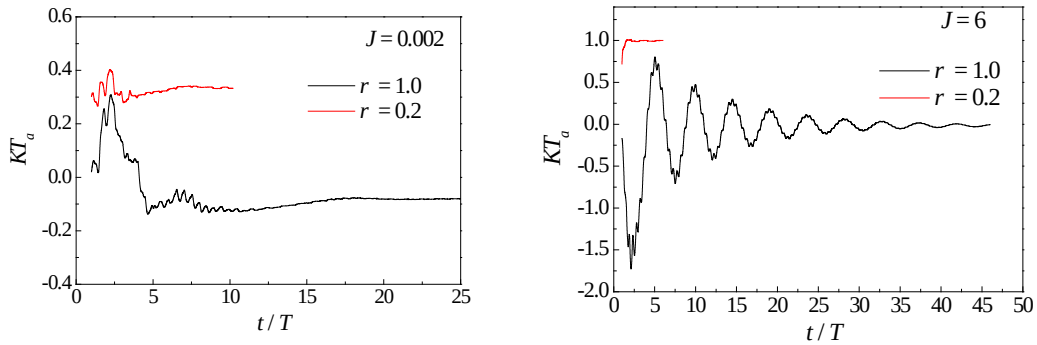

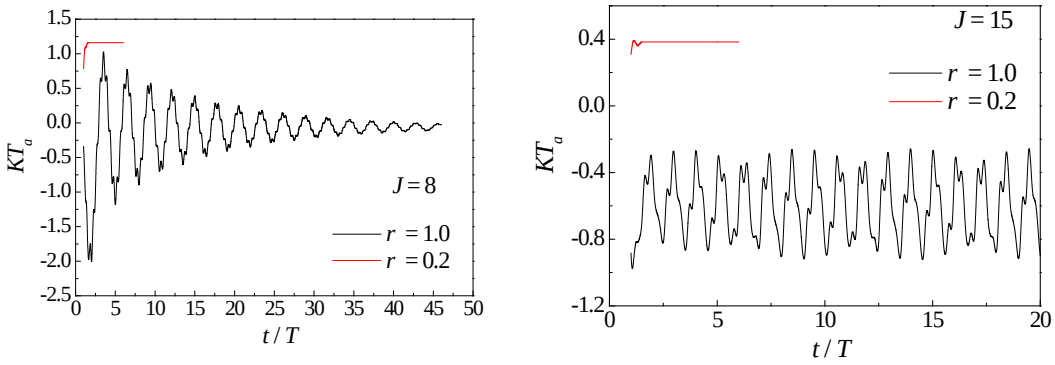

Figure12. Short-time average thrust coefficient curves with and without resonance at different advance coefficients

It can be seen from Fig. 12 that under the condition of frequency ratio r = 1, i.e. resonance state, the curves of short-term average thrust coefficient KT_a under different working conditions shows great fluctuation. Under the condition of J=0.002, the curve of KT_a tends to be stable after 18 cycles, but the average value is negative; under the condition of J=6 and J=8, KT_a shows gradual convergence fluctuation, which tends to 0 value finally; under the condition of J=15, KT_a curve shows a certain amplitude fluctuation, but the average value is still negative. From the above results, the SPFF can not provide effective thrust when the system resonates, so the system parameters should be designed far away from the resonance point of the system, which is consistent with the conclusion of Thaweewat (2018). In contrast, when r= 0.2, all the average thrust coefficient KT_a curves are relatively stable. When J= 0.002, the thrust becomes stable after about7 cycles; In other cases, the thrust of the foil tends to be stable after only 2 to 3 cycles.

In order to further explain the problem that the SPFF can not provide stable thrust in the case of system resonance, through the analysis of AOA α and pitching angle θ, we speculate that there are two main reasons. The first reason is that, the pitching angle θ is too large caused by system resonance, which leads to the AOA increases abruptly. As shown in Fig.13 (a), under the condition of J = 0.002, i.e. close to the start-up state of the system, the maximum pitching angle θ reaches as high as 110°， and the AOA curve appears step change. The reason for AOA curve step may be that when the advance speed V_A is too small, the relative velocity angle of the foil will change abruptly. Another reason why the SPFF system can not produce stable thrust is that the system can not form a good adaptive pitching angle under the effect of system resonance, which can be divided into two cases. In the first case, as shown in Fig. 13(a), the pitching angle θ is close to zero at the complete alternation. While, the ideal self-pitching flapping angle should reach the extreme value at the at the complete alternation time. Because the flapping foil is at the center line of heave motion at that time, the heave motion speed V_y and the torque generated both reach the maximum; The second case is, as shown in Fig.13(b), at the complete alternation time, the pitching angle θ is close to the extreme value, but the AOA α is close to zero, which means that the force on the flapping foil is very small, and the ideal case is the pitching angle and the AOA is in the same phase so that the lift cccould produces the maximum thrust in the forward direction.

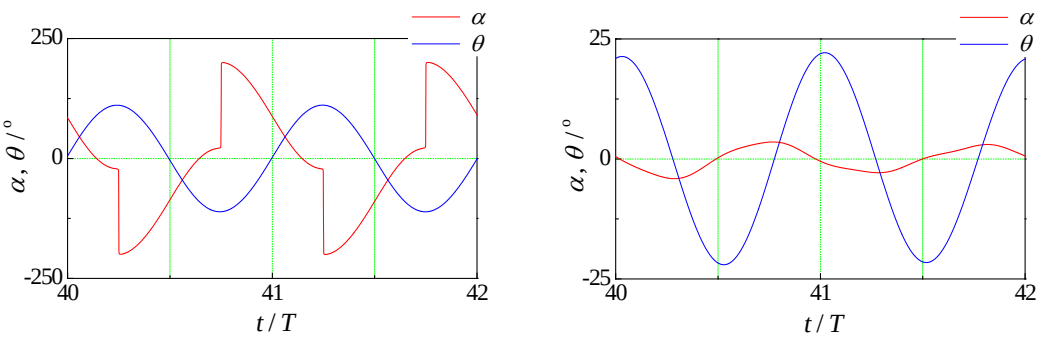

J=0.002 *J*=8

Figure 13. The curves of pitching angle and AOA at *J* = 0.002 and *J*= 8 working condiction under system resonance state

Then, in order to further study the influence of frequency ratio on the performance of the SPFF, the foil performance under six frequency ratios is further analyzed. The selected six frequency ratios are 0.01, 0.2, 0.5, 0.8, 1.5, and 2.0. The frequency ratio of SPFF is set by adjusting the moment of inertia of the foil. The short-term average thrust coefficient curve and pitching angle curve of SPFF under J = 8 working condition at r = 1.0, 1.5 and 2.0 are shown in Fig.14. It appears that the results of *r*=1.5 and 2.0 are similar to the resonance case of *r*=1.0, pitching angle θ is large, and the force on the flapping foil is resistance. And when the frequency ratio is greater than 1.0, the correlation between the force on the foil and the frequency ratio is not clear. Since this phenomenon should be avoided in practical application, the case of frequency ratio greater than 1 will not be discussed later in this paper.

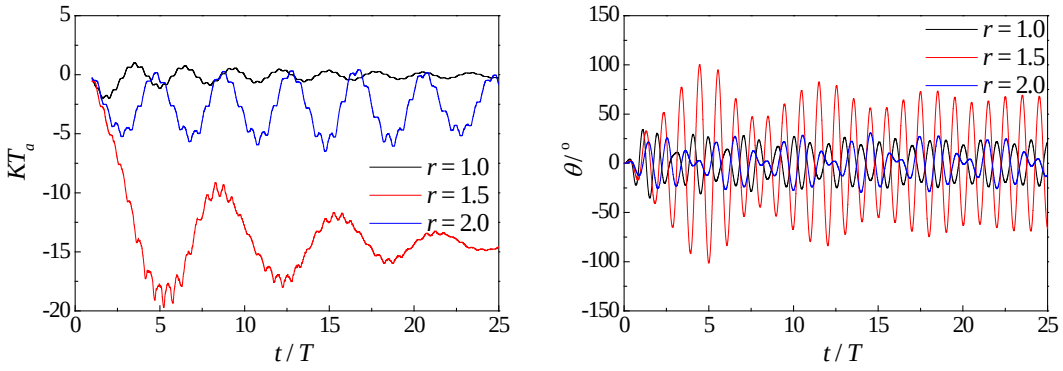

(a) Short-time average thrust coefficient curve (b) pitching angle curve

Figure14. Time- history curves of foil performnce at *J*=8 working condition at three frequency ratios

The foil performance at other four frequency ratios (*r*=0.01, 0.2, 0.5 and 0.8) are shown in Fig.15. It can be seen that the performance curves at *r*=0.01 and *r*=0.2 are almost coincident, which indicates that the effect of frequency ratio on the performance of foil can be ignored at a small frequency ratio. When the frequency ratio increases from 0.2 to 0.5, there is almost no change in the maximum efficiency of the foil; The efficiency curve on the left side of the maximum efficiency point slightly increases, while the curve on the right side slightly decreases; The thrust coefficient curve also presents a similar law. When the frequency ratio increases from 0.5 to 0.8, the change of efficiency curve is similar to that of the former. The curve on the left side of the highest efficiency point increases, while the curve on the right side decreases; The difference is that the thrust curve decreases obviously; In addition, when the frequency ratio is at 0.8, the thrust coefficient curve begins to show irregular pulsation, which may be caused by the fluctuation of short-term average thrust coefficient. To verify this conjecture, Fig.16 shows the time-history curves of short-term thrust coefficients for *J* = 4 and *J* = 10 with frequency ratio of 0.8. It can be seen from the results that there is a large range of thrust coefficient fluctuation under these both conditions. The thrust coefficient curve shows continuous fluctuation under *J* = 4 condition; The curve fluctuation under *J* =10 condition shows a convergence trend, but the convergence is extremely slow. The reason for this fluctuation phenomenon may be that, the SPFF system is very close to the resonance state when frequency ratio is at 0.8, .

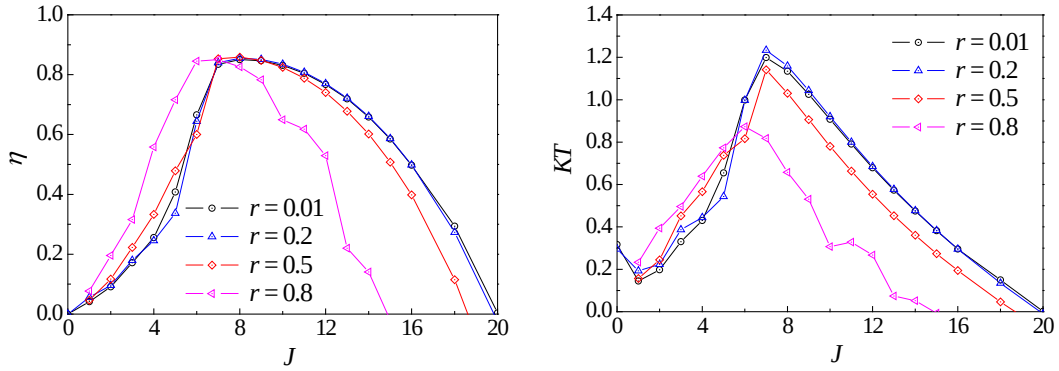

Figure 15. Thrust and efficiency curves at four different frequency ratios

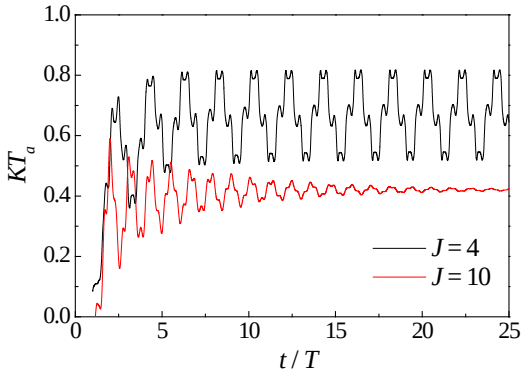

Figure16. Short-time thrust coefficient time-history curves under two working conditions (r=0.8, J=4 and J=10)

In summary, the existing results show that the SPFF can not provide effective thrust when the system resonates, so the parameters should be designed far away from the resonance state of the system; At the same time, in order to form a better self-pitching angle, the smaller frequency ratio should be selected as far as possible. According to the definition of frequency ratio, a smaller frequency ratio means that the foil moment of inertia is smaller, that is to say, the follow-up performance of the foil is better, and a more favorable self-pitching angle could be formed; On the contrary, a larger frequency ratio will result in a larger pitching angle θ or an unreasonable AOA of the foil, which makes the SPFF system unable to output thrust normally. Considering that a smaller frequency ratio means a smaller moment of inertia or a larger spring stiffness, which may be difficult to achieve in engineering, a more moderate frequency ratio r=0.2 is selected for correlation analysis in this paper.

5.2 Pitching motion analysis

Due to torsion spring attached to the foil, the pitching motion of SPFF is very complex and its influence parameters are more than that of conventional flapping foil. However, if the frequency ratio of SPFF is small, i.e. the foil moment of inertia is small, the pitching motion of the foil is mainly affected by the spring stiffness ratio and hydrodynamic moment. In this section, the influence of spring stiffness ratio K' on the performance of SPFF and the characteristics of pitching motion will be discussed first. Subsequently, the position of the pitching center which has a great influence on the hydrodynamic moment is analyzed. And its influence on the pitching motion characteristics is further analyzed.

5.2.1 Effect of spring stiffness ratio

In this part, the effect of the spring stiffness ratio K' on the performance and pitching motion of SPFF is discussed at a lower frequency ratio r = 0.2. The comparison results of the performance curves of the SPFF

with 0.1, 1.0, 10.0 and 100.0 spring stiffness ratios are shown in Fig. 17. Different spring stiffness ratios *K'* are realized by adjusting the spring stiffness. In order to keep the frequency ratio constant, the foil moment of inertia should be adjusted accordingly.

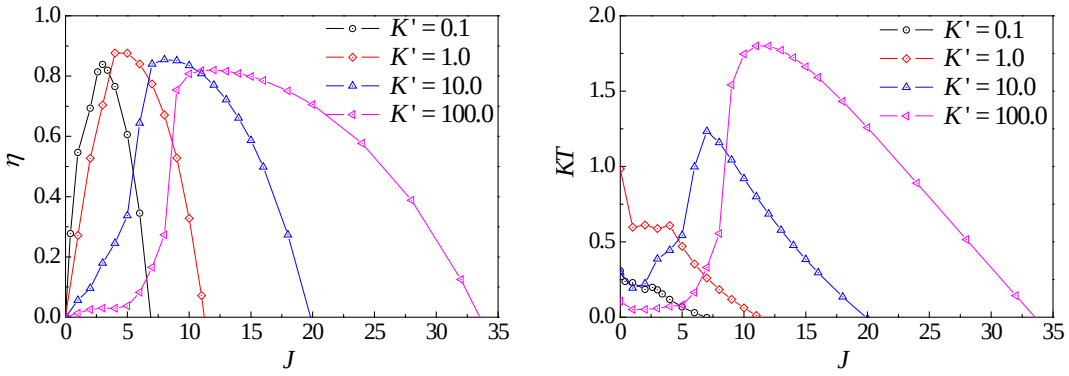

（a）Propulsive efficiency　　（b） Thrust coefficient

Figure 17. Propulsive performance with different spring stiffness ratios

Firstly, from the results shown in Fig.17(a), the SPFF can work efficiently over a wide range of spring stiffness ratios, and the maximum efficiency with the four different spring stiffness ratios all exceeds 80%. In the case of K'=1.0, the maximum efficiency reaches 87.6%, which is very close to that achieved by Thaweewat (2018). The results given by Thaweewat (2018) are contour diagrams, the definitions of spring stiffness ratio and advance coefficient are also different from those given in this paper. After estimating the highest efficiency point of the contour diagram in Thaweewat' work and converting relevant parameters, the highest efficiency point in literature is located at the working condition of r=0.19, K'=0.44, J=3.53, which is very close to the highest efficiency working condition in this paper. Secondly, as shown in Fig.17 (a), the highest efficiency on the performance curve first increases and then decreases as the spring stiffness ratio increases. But on the whole, the gap among these foil highest efficiency with different spring stiffness ratios is not big. However, with the increase of spring stiffness ratio of SPFF, the high efficiency working range of foil increases obviously, and the advance coefficient that can be achieved also increases gradually. In the case of K'=100.0, the SPFF can work at a high efficiency with a larger range of advance coefficient. For example, in a wide range of working conditions where the advance coefficient is from 10 to 20, the efficiency of the SPFF could be kept above 70%. However, when the spring stiffness ratio is small, such as K' = 0.1, the SPFF could generate thrust in a small range of working conditions where the advance coefficient is from 0 to 7. In addition, it can be seen in Fig. 17 (a) that the efficiency curve characteristics of the foil at low advance coefficient change with the change of the spring stiffness ratio. When the spring stiffness ratio is small, the efficiency increases rapidly with the increase of the advance coefficient; However, with a larger spring stiffness ratio, there is a large range of advance coefficient, and the efficiency remains low. However, on the whole, there is a sudden rise in the efficiency curve on the left side of the highest efficiency point, which is due to the transition of the foil from the flow separation working state to the non separation working state.

It can be seen from the results shown in Fig. 17 (b) that the foil thrust curve characteristics with different spring stiffness ratios are quite different. In the case of K'= 0.1 and K' = 1.0, the thrust coefficient curve decreases monotonously with the advance coefficient. When k'= 10.0 and K' = 100.0, the thrust coefficient curve has a low valley at low advance coefficient and a peak near the maximum efficiency point. At the same time, it is found that the right half of the thrust coefficient curve shifts to the upper right with the increase of the spring stiffness ratio, that is to say, the larger spring stiffness ratio can provide higher thrust at higher advance coefficient; At the beginning of the thrust coefficient curve, that is, in the foil start-up state, the maximum thrust coefficient appears in the case of K'= 1.0. Regardless of the spring stiffness ratio, the thrust coefficient in the start-up state decreases gradually with the advance coefficient.

To sum up, from the performance curve of the flapping-foil under different spring stiffness ratio, there is a dilemma in the selection of the SPFF spring stiffness ratio. For a flapping-foil propeller, the spring stiffness and moment of inertia are determined if the design has been finalized. When the pitching frequency and amplitude are constant, it is difficult to work at a higher advance coefficient if a smaller spring stiffness ratio K' is used to achieve a higher thrust in the starting state; On the contrary, if a larger K' is used to achieve high thrust and high efficiency at high advance coefficient, the thrust at starting state will be small, starting will be difficult with poor maneuverability. However, from the definition of spring stiffness ratio, different spring stiffness ratios can be obtained by changing the pitching frequency and amplitude in order to achieve high performance in various working states. Since the spring stiffness ratio is inversely proportional to the square of the pitching frequency and the third power of the pitching amplitude, the decrease of the spring stiffness ratio will be very obvious. At the same time, the thrust is proportional to the square of the pitching frequency and the third power of the pitching amplitude, so the increase of the thrust is also very obvious. According to the above analysis, a design idea can be provided. The SPFF could be designed with a higher spring stiffness ratio. When a larger thrust is required, for example, in the starting state, the spring stiffness ratio of the system can be reduced by increasing the pitching frequency and amplitude, thus a larger thrust can be obtained. The minimum moment of inertia design could be used to achieve a smaller frequency ratio. This is just a qualitative discussion. For a real vehicle, more detailed propeller parameter design is required based on its drag characteristics.

In addition to the propulsion efficiency, the spring stiffness ratio also affects the pitching angle and AOA of the flapping-foil. However, since the pitching angle and AOA vary periodically, only the maximum pitching angle and AOA of each working condition are analyzed here. Fig.18 shows the maximum pitching angle and maximum AOA of foil with different spring stiffness ratios. Obviously, as the spring stiffness ratio increases, the maximum pitching angle curve of the flapping-foil shifts to the lower left, as shown in Fig.18(a). This is because the larger the spring stiffness ratio is, the smaller the pitching angle produced by the hydrodynamic moment is. That is, the spring stiffness ratio could be used to measure the pitching angle. It can be seen from Fig.18(b) that with the increase of spring stiffness ratio, the maximum AOA curve is gradually shifted to the upper right. This is also easy to understand, because with the increase of the spring stiffness ratio, the hydrodynamic moment that the spring can resist is increasing, and the hydrodynamic moment increases with the increase of theAOA. As a result, the AOA of the foil is increasing. It is also found in Fig.18(b), when the spring stiffness ratio is small, the maximum AOA does not change much; as the spring stiffness ratio increases, the maximum AOA increases gradually. With different spring stiffness ratio, the foil maximum AOA corresponding to the highest efficiency point are mainly concentrated at about 15°.

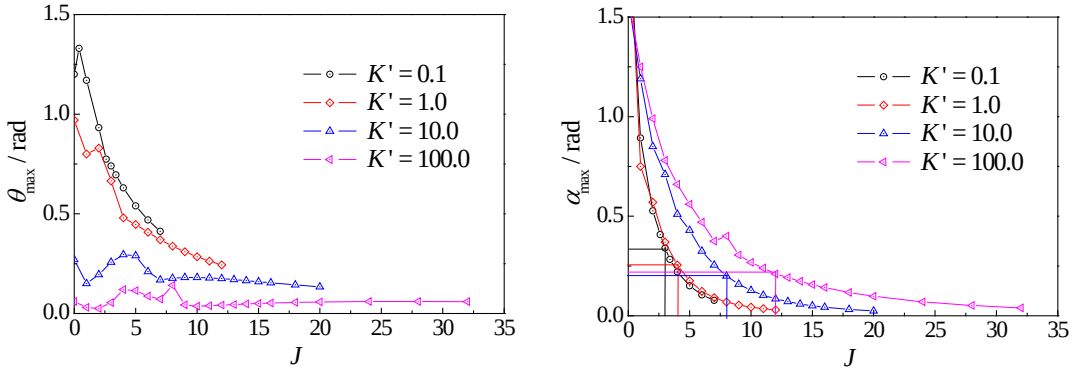

（a）Maximum pitching angle　　（b）Maximum angle of attack

Figure 18. Maximum pitching angle and angle of attack with different spring stiffness ratios

5.2.2 Effect of pitching center position

Under the condition of k'=10.0, the flapping-foil performance and pitching motion with different pitching center positions are analyzed. The three selected pitching center positions c_0 are -0.1c, 0, and 0.1c. The definition of c_0 is shown in Fig.2 and its direction is positive towards the trailing edge of the foil. The performance comparisons of different pitching center positions are shown in Fig.19. In order to compare with Fig.17, the performance curves with different spring stiffness ratios are also retained in Fig.19. It can be seen from the figure that the variation trend of the flapping-foil performance curves at different pitching center positions is approximately close to that with different stiffness ratios. When pitching center position shifts to the trailing edge, the hydrodynamic arm will be smaller, thus the hydrodynamic moment will become smaller and the pitching angle will be reduced. As discussed earlier, the reduced pitching angle is equivalent to the increase of spring stiffness ratio, so the performance curve moves towards the direction of a larger spring stiffness ratio when the pitching center position shifts to the trailing edge, and vice versa. When the center position moves to the outside of the leading edge, i.e. c_0=-0.1c, the efficiency increases slightly, which is also close to the effect of spring stiffness ratio. Compared with c_0=0.1c, the efficiency is increased by about 1.2 percentage points. In engineering project, a negative center position can be achieved by additional brackets. Finally, the changes of the maximum pitching angle and the maximum AOA curves with different pitching center positions are analyzed, as shown in Fig. 20. For comparison with Fig.18, the curves under different spring stiffness ratios are still retained. It can be seen from Fig. 20(a) that when c_0 increases, the hydrodynamic moment decreases and the maximum pitching angle decreases with the increase of C_O, which is consistent with the influence of spring stiffness ratio. But in the range of J = 3 ~ 6, the pitching angle amplitude increases suddenly, which may be caused by the violent pitching angle fluctuation. We could try to increase the damping of the spring system to reduce the pitching angle oscillation. The variation law of the maximum AOA to the different pitching center positions is similar to that in Fig.18(b). When c_0 increases, the hydrodynamic moment decreases and the maximum AOA increases.This result further indicates that the influence of pitching center position on the maximum AOA and pitching angle curve is basically consistent with that of spring stiffness ratio.

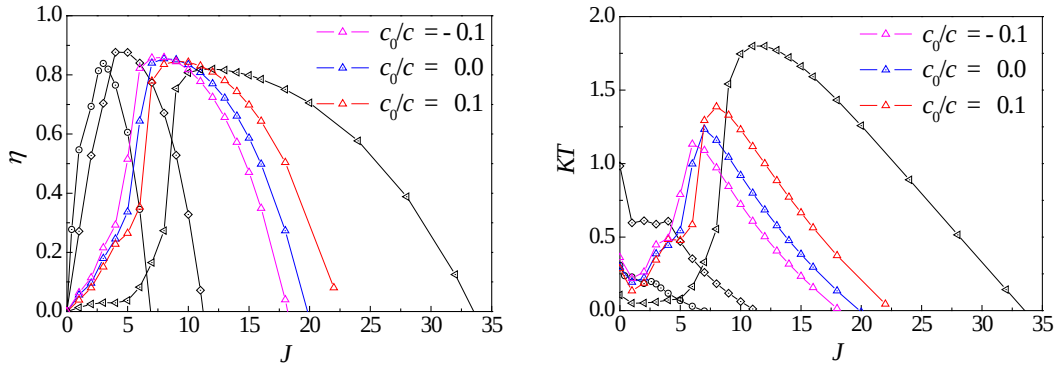

（a） Propulsive efficiency　　（b） Thrust coefficient

Figure19. performance with different pitching center positions

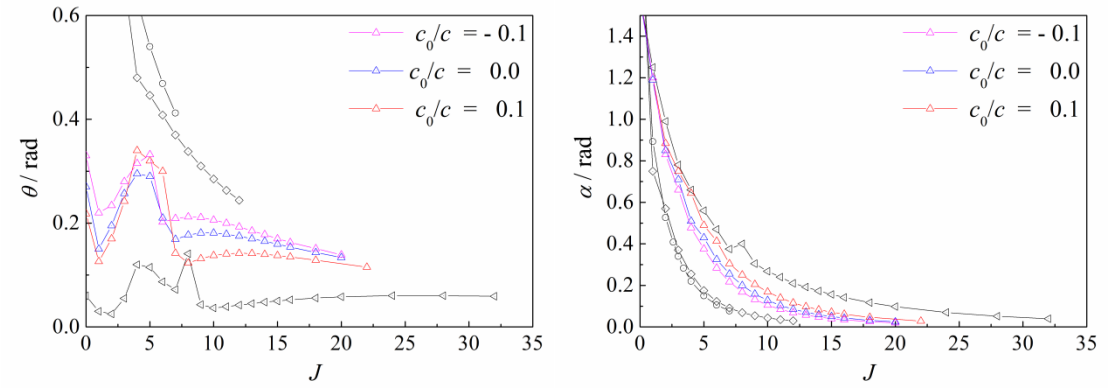

（a）Maximum pitching angle　　（b）Maximum AOA

Figure 20. Maximumpitching angle and MaximumAOA with different pitching center positions

6. CONCLUSIONS

The propulsion performances of a self-pitching flapping foil are investigated systematically in this work. The foil heave motion is accurately prescribed by a simple harmonic function whereas the pitch motion is passively induced by an attached torsion spring system. The fluid-structure coupling method is used to analyze the working characteristics of the self-pitching flapping foil with different parameter settings. All the numerical simulations under each parameter setting are completed under the integral working condition from the advance coefficient of 0 to the foil thrust of 0.

1. The poor repeatability of performance parameters in the low advance coefficient range (J = 2 ~ 6) is due to the large angle of attack and unstable separation onthe surface of foil.

2. The analysis of different frequency ratio shows that the system resonance will make the foil deviate from the ideal angle of attack, and the propulsion performance of the system will decline or even lose the propulsion ability; When the frequency ratio is small, that is, the foil has a small moment of inertia, the self-pitching flapping foil can work well, and the maximum efficiency could reach as high as 86% ; The more suitable frequency ratio could be selected below 0.5.

3. The research on the spring stiffness ratio shows that if a small frequency ratio is selected, the self-pitching flapping foil can work normally in a very large range of spring stiffness ratio, which is up to 0.1 ~ 1000 in this paper. Moreover, the peak efficiency under different spring stiffness ratios is not monotonic, and there is a maximum value. When k'= 1.0, the highest efficiency could reache 87.6%.

4. With the increase of the spring stiffness ratio, the wide efficiency working range of the foil increases obviously, and the advance coefficient that can be achieved also increases gradually. That is to say, the change of thrust under different working conditions could be realized by adjusting the spring stiffness ratio, flapping frequency and amplitude.

5. Through the analysis of the performance curves of the foil with different pitching center positions, it is shown that the influence trend of the pitching center position is close to that of the spring stiffness ratio. When the position of the pitching center deviates to the trailing edge, the hydrodynamic arm will be smaller, so the hydrodynamic moment will be smaller and the pitching angle of the foil will become smaller, which is equivalent to the increase of the spring stiffness ratio. So the performance curve will deviate to the direction of the larger spring stiffness ratio.

ACKNOWLEDGEMENTS

This work received funds from National Natural Science Foundation of China (Grant No. 51309070, 51503051), Shandong Province Science and technology development plan item (Grant No. 2013GGA10065).

REFERENCES

Andersen, A., et al., (2017). Wake structure and thrust generation of a flapping foil in two-dimensional flow. Journal of Fluid Mechanics, 812.

Anderson, J. M. , Streitlien, K. , Barrett, D. S., and Triantafyllou, M. S.. (1998). Oscillating foils of high propulsive efficiency. Journal of Fluid Mechanics, 360, 41-72.

Bøckmann, E. and Steen,S. (2014). Experiments with actively pitch-controlled and spring-loaded oscillating foils. Applied Ocean Research, 48, 227-235.

Boudreau, M., et al., (2018). Experimental investigation of the energy extraction by a fully-passive flapping-foil hydrokinetic turbine prototype. Journal of Fluids and Structures,82, 446-472.

Bourlet, T. F., Gurugubelli, P. S., and Jaiman, R. K.. (2015). The boundary layer development and traveling wave mechanisms during flapping of a flexible foil. Journal of Fluids and Structures, 54, 784-801.

Cleaver, D.J., et al., (2016). Lift enhancement through flexibility of plunging wings at low Reynolds numbers. Journal of fluids and structures,. 64: p. 27-45.

Dewey, P.A., et al., (2013). Scaling laws for the thrust production of flexible pitching panels. 29-46.

Esfahani, J.A., Barati, E. and Karbasian, H.R. (2015). Fluid structures of flapping airfoil with elliptical motion trajectory. Computers & fluids, 108, 142-155.

Floc'h, F., Phoemsapthawee, S. , Laurens, J. M. , and Leroux, J. B. (2012). Porpoising foil as a propulsion system. Ocean Engineering, 39(none), 53-61.

Floryan, D., Buren, T. V., Rowley, C. W., and Smits, A. J.. (2017). Scaling the propulsive performance of heaving and pitching foils. Journal of Fluid Mechanics, 822.

Gritskevich, M.S., et al., (2012).Development of DDES and IDDES Formulations for the k-ω Shear Stress Transport Model. Flow, Turbulence and Combustion, 88(3): p. 431-449.

Guglielmini, L., and Blondeaux, P.(2004). Propulsive efficiency of oscillating foils. European Journal of Mechanics, B/Fluids, 23(2), 255-278.

Hoppe, K G. (1989). The dynamo-elastic oscillating foil propeller. Schiff Und Hafen, 41.

Joe, H., et al.,(2017). Development of a flap-type mooring-less wave energy harvesting system for sensor buoy. Energy, 133,851-863.

Karbasian H.R., Esfahani J.A., (2017). Enhancement of propulsive performance of flapping foil by fish-like motion pattern, Computers & Fluids, 156, 305-316

Kim, D., Strom, B., Mandre, S., Breuer, K., (2017). Energy harvesting performance and flow structure of an oscillating hydrofoil with finite span. J. Fluids Struct. 70, 314– 326.

Koochesfahani, Manoochehr M.(1989). Vortical patterns in the wake of an oscillating airfoil. Aiaa Journal, 27(9),1200-1205.

Lee, N. , Lee, S. , Cho, H., and Shin, S. J.. (2018). Effect of flexibility on flapping wing characteristics in hover and forward flight. Computers & Fluids.

Li, M.Y.(2019). Flow Mechanism Analysis And Experimental Study Of Swing Wing Propulsion. Master's thesis, Harbin Institute of Technology.

Lin, X., Wu, J., and Zhang, T.. (2019). Performance investigation of a self-propelled foil with combined oscillating motion in stationary fluid. Ocean Engineering, 175, 33-49.

Menter F. R. and Rumsey L., (1994)."Assessment of two-equation turbulence models for transonoc flows," in AIAA 25th Fluid Dynamics Conference, AIAA Paper 94-2343, (Colorado Springs, CO), June

Read, D. A., Hover, F. S., and Triantafyllou, M. S..(1989). Forces on oscillating foils for propulsion and maneuvering. Journal of Fluids & Structures, 17(1), 163-183.

Schnipper, T., Andersen, A., & Bohr, T.. (2009). Vortex wakes of a flapping foil. Journal of Fluid Mechanics, 633, 411.

Schouveiler, L. , Hover, F. S., and Triantafyllou, M. S. (2005). Performance of flapping foil propulsion. Journal of Fluids and Structures, 20(7), 949-959.

Taylor, G.K., Nudds R.L. and Thomas, A.L.R. (2003）. Flying and swimming animals cruise at a Strouhal number tuned for high power efficiency. Nature, 425(6959): p. 707-711.

Teng, L., et al. (2016).Effects of non-sinusoidal pitching motion on energy extraction performance of a semi-active flapping foil. Renewable Energy, 85: 810-818.

Thaweewat, N., Phoemsapthawee S. and Juntasaro V. (2018). Semi-active flapping foil for marine propulsion. Ocean Engineering, 147, 556-564.

Veilleux, J. and Dumas G. (2017).Numerical optimization of a fully-passive flapping-airfoil turbine. Journal of Fluids and Structures, 70, 102-130.

Wu, X., et al. (2020). A review on fluid dynamics of flapping foils. Ocean Engineering, 195, 106712.

Yang, F., et al.(2018). Numerical investigation of a wave glider in head seas. Ocean Engineering, 164, 127-138

Zhang, X. , Su, Y. M., and Wang, Z. L.. (2012). Numerical simulation of the hydrodynamic performance of an unsymmetrical flapping caudal fin. Journal of Hydrodynamics, Ser. B, 24(3), 354-362.